Journal of Fundamental and Applied Research **Vol. 5**, Issue 4 (2025) **20250031**

Received: 10 November 2025 / Accepted: 24 December 2025
Published online: 25 December 2025
© 2025 The Author(s)

Effect of the spark discharge method in an electrolytes medium on the stoichiometry of Ni-Ti-V-Zr-Nd system nanoparticles

A.A. Zaripov[1,*] and Kh.B. Ashurov[1]

[1]*Arifov Institute of Ion-Plasma and Laser Technologies, Academy of Sciences of the Republic of Uzbekistan, 33 Durmon Yuli St., 100125, Tashkent, Uzbekistan*

Abstract. In this study, complex nanocomposite particles of the Ni-Ti-V-Zr-Nd system were synthesized using the spark discharge method in an aqueous NaCl electrolyte. XRD analysis revealed that the material consists of a highly crystalline intermetallic core (Ni-Ti B2 and Ni_3Ti phases), with Nd and Zr dopants forming a solid solution and creating lattice microstrains. Raman spectroscopy (132, 159, and 443 cm^{-1}) confirmed the presence of a stable oxide shell on the nanoparticle surface, proving the formation of a "core-shell" structure. The preservation of all alloying elements proves that the inter-element stoichiometric balance was successfully maintained.

Key words: aNi-Ti-V-Zr-Nd alloy; spark discharge; XRD; Raman spectroscopy; stoichiometry; nanoparticles; core-shell.

I. INTRODUCTION

Alloys that incorporate elements with different atomic radii, such as Nd and Zr, into Ti and Ni lattices, thereby creating strong lattice distortions, belong to the category of Complex Concentrated Alloys (CCA) [1]. In this context, strong distortions in the crystal lattice occur due to phase transformations [2]. According to studies of such complex Ni-Ti-V-Zr-Nd alloy systems, the "high entropy effect" ensures phase stability and promotes the formation of complex intermetallics [3, 4]. These alloying elements, Zr and V, enter the Ni-Ti lattice, increasing its corrosion resistance and reducing crystallite size [5]. Nd, as a rare earth element (REE), accumulates at the grain boundaries and reduces the agglomeration of nanoparticles, thereby increasing stability according to DLVO theory [6]. However, in the presence of high-charge Nd and Zr ions, compression of the electrical double layer (EDL) may occur. As a reason for this, the classics of DLVO theory point out that under conditions where the zeta-potential of the system is insufficient, Van der Waals forces prevail [7].

However, synthesizing Ni-Ti-based multi-component nanoparticles is considered one of the most complex tasks in materials science. The main problem in this process is the differing melting temperatures and oxidation tendencies of the components. For example, the Spark Discharge method is based on obtaining nanoparticles through a plasma discharge between metal electrodes. Although it offers high purity and the possibility of obtaining nanoparticles from complex alloys in a single step, the composition of the nanoparticles may differ from the electrode composition—breaking the stoichiometry—due to the varying evaporation rates of elements like Ni and Ti under the spark [8]. Similarly, in creating mechanical alloys through the Planetary Ball Milling method, Ni, Ti, V, Zr, and Nd powders are ground in high-energy mills for long periods. While this method is convenient for obtaining large volumes of powder, long-term milling leads to elements mixing at the atomic level to form a "solid solution". This results in material contamination from the milling balls and walls, as well as an extremely wide size distribution of particles [9]. Furthermore, while the Laser Ablation in Liquids method is very effective for obtaining "Core-Shell" structures covered with a surface oxide layer, it leads to a decrease in productivity due to the absorption of laser energy by the liquid [10]. Although Sol-Gel and chemical reduction methods allow for the production of extremely small (< 10 nm) particles, it is very difficult to reduce elements like Ti and Zr in an aqueous medium. This is because they are highly active metals that oxidize immediately to form hydroxides. For the Ni-Ti system, this method usually yields low-quality results [11].

Based on the comparative analysis above, employing the spark discharge method in a dielectric liquid medium is the most optimal approach for multi-component systems such as Ni-Ti-V-Zr-Nd [8, 11]. However, at present, maintaining stoichiometric

* Corresponding author: zaripov@iplt.uz

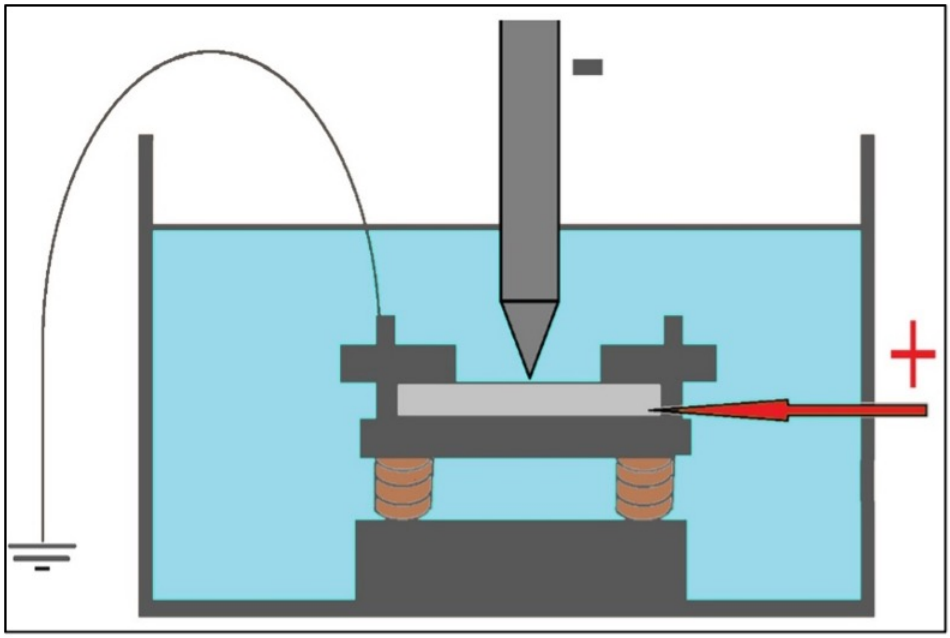


FIG. 1: Schematic view of the apparatus

balance remains a pressing issue due to the diverse physical properties of the components [12]. In this paper, as a solution to the problem, the synthesis of multi-component Ni-Ti-V-Zr-Nd nanoparticles with preserved stoichiometry is proposed by applying the spark discharge method in aqueous NaCl electrolytes.

II. METHODS AND APPARATUS

Figure 1 presents a schematic diagram of the experimental setup designed for the synthesis of metal and alloy nanoparticles using the spark discharge method. The apparatus configuration includes a conical cathode and a cylindrical anode with a diameter of 2 mm, both fabricated from the target material and positioned vertically opposite each other along the same axis. The technical implementation of the setup is based on an original pulsed power supply unit assembled using high-speed, high-voltage IRG4PH50UD IGBT switches and 150EBU04 diodes. The control circuit allows for flexible adjustment of the synthesis parameters: operating voltage up to 450 V, current intensity up to 10 A, and pulse repetition frequency up to 30 kHz. To initiate a stable spark discharge and ensure the effective dispersion of the multi-component alloy, the anode was completely submerged in the electrolyte, while the immersion depth of the conical cathode was varied within a range of 1 to 8 mm. During the process, a continuous circulation of the working fluid was maintained, which facilitated the thermostatting of the reaction zone and ensured the timely removal of erosion products from the inter-electrode gap, preventing their re-melting or coagulation. During the experiments, a direct current (DC) voltage of up to 250 V was supplied to the unit, while the control system ensured the generation of pulses with a frequency of up to 30 kHz. Throughout the operation, the current intensity was maintained at a level of up to 1 A, allowing for the preservation of a stable spark discharge mode.

To prepare the working fluid a 1% electrolyte analytical grade (”CCH” grade, GOST 4233-77) NaCl salt and distilled water were utilized. All weighing procedures were performed using analytical balances with a precision of ± 0.001 g. The electrolyte concentration was experimentally optimized, when the salt content was less than 1%, instability in the initiation of the spark discharge was observed, whereas exceeding this threshold led to an increase in parasitic electrochemical processes. The employment of a pulsed high-frequency mode allowed for the localization of the impact within the spark channel zone, thereby minimizing the contribution of electrolysis to the formation of the final products. The phase composition and crystal lattice parameters of the resulting multi-component composite nanoparticles were investigated by X-ray diffraction (XRD) using a Rigaku RD-6100 diffractometer. To analyze the crystalline structure and symmetry of the nanoparticles, Raman spectroscopy was employed using an InVia Raman spectrometer (Renishaw). For the experiments, nanoparticles obtained by dispersing a Ni-Ti-V-Zr-Nd alloy, comprised of Ni (71.17%), Ti (18.83%), V (3.57%), Zr (2.34%), and Nd (2.29%) under the influence of spark discharges in an electrolyte were used as samples.

 Copyright © 2025

III. EXPERIMENTAL RESULTS

The concentration of the NaCl electrolyte was maintained at a specific molarity to optimize the medium's electrical conductivity. The presence of Na^+ and Cl^- ions ensures a stable plasma channel formation during the spark discharge. High ionic conductivity localizes the discharge energy, increasing the instantaneous power density. This facilitates the simultaneous thermal erosion of all alloying elements (Ni, Ti, V, Zr, Nd), regardless of their individual melting points, which is a key factor in maintaining the stoichiometric consistency of the synthesized multi-component nanoparticles.

Figure 2 presents an optical image of the Ni-Ti-V-Zr-Nd nanoparticles, which allows for a visual assessment of the synthesized nanopowder structure.

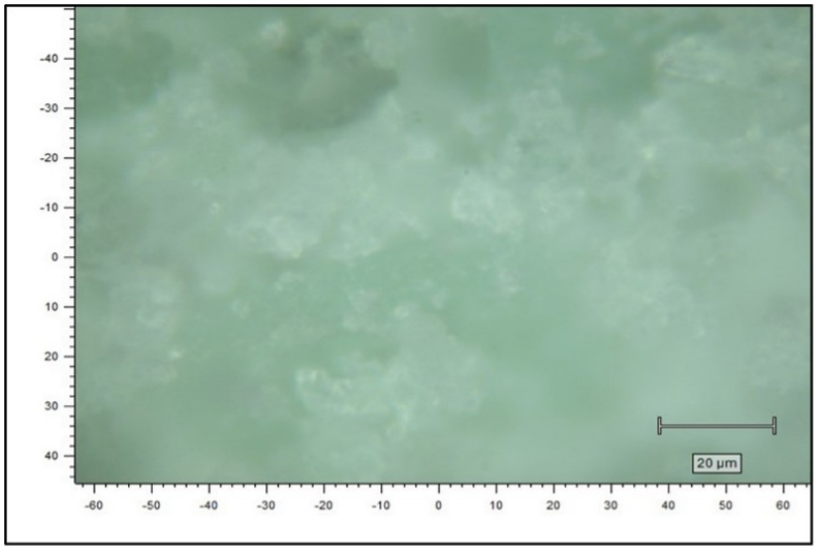


FIG. 2: Optical image of the sample

In this image with a 20 μm scale, the light green-blue tint indicates the presence of nickel compounds, specifically nickel hydroxide or oxide, within the sample. The powder consists of various-sized agglomerates formed by the mutual adhesion of submicron-sized nanocrystals. The 20 μm scale illustrates the average granularity of the sample. The phase analysis of this sample clarifies its properties even more precisely. For this purpose, the XRD analysis is presented in Figure 3 below.

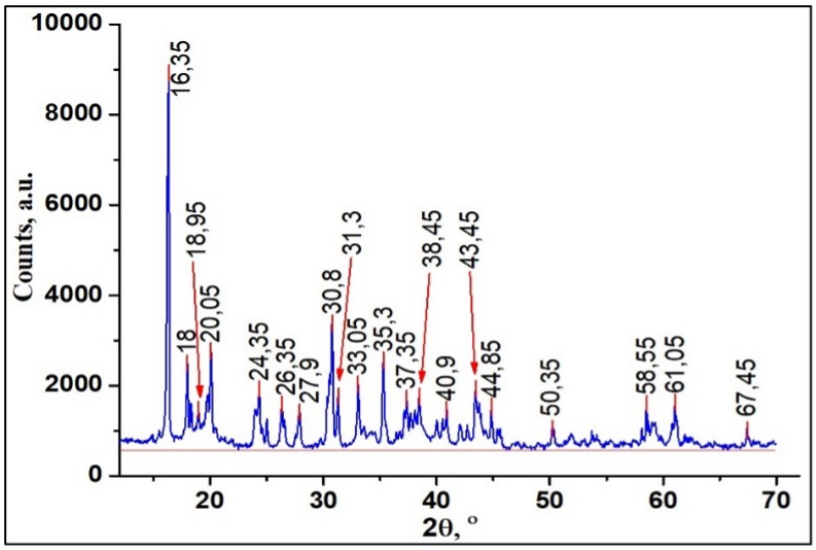


FIG. 3: XRD analysis of the sample

This XRD spectrum possesses an exceptionally complex and rich structure. While the high concentration of Ni (71.17%) and Ti (18.83%) defines the primary phases, the V (3.57%), Zr (2.34%), and Nd (2.29%) additions have altered the symmetry of the

Copyright © 2025

crystal lattice, leading to the emergence of new peaks. Below is a comprehensive and systematic interpretation of all identified peaks.

In the low-angle dominant region, specifically $2\theta = 16^\circ - 20^\circ$, typical metal alloys usually do not exhibit any peaks. However, in this sample, the primary peak is observed at 16.35°, representing the phase with the highest intensity. These are super-lattice intermetallic clusters based on Nd-Ni or Zr-Ni, characterized by a large lattice constant. Due to the large atomic radius of Nd, it can form such new structures at these small angles [13]. The peaks at 18.0°, 18.95° and 20.05° are satellite peaks of the main phase, indicating a low-symmetry system, such as orthorhombic or monoclinic. This is a direct result of the intense lattice deformation caused by the integration of Nd and Zr into the Ni-Ti matrix.

In the mid-angle diffusion region $2\theta = 24^\circ - 38^\circ$, various compounds of Ti and the alloying elements are situated. The peaks at 24.35° and 26.35° are close to complex oxides such as TiO_2 (anatase) or $ZrTiO_4$ type. This, in turn, indicates that surface oxidation of the nanoparticles occurred during the synthesis process. The peaks at 27.9°, 30.8° and 31.3° within this group correspond to $NiZr_2$ or Ni_2V phases. The V and Zr in the composition demonstrate their crystallinity precisely in this region. Furthermore, the peaks at 33.05°, 35.3° and 37.35° are reflections from various crystallographic planes of the Ni_3Ti (hexagonal) phase. Since the nickel content exceeds 70%, the formation of Ni_3Ti is thermodynamically inevitable.

The high-angle metallic region, specifically the $2\theta = 38^\circ - 45^\circ$ section, represents the primary metallic phases that ensure the mechanical strength of the material. The peaks at 38.45° and 40.9° belong to V_2O and NiO. The peaks at 43.45° and 44.85° are considered the "heart" of the system. The overlapping of the Ni-Ti (austenite B2 phase) and NiO lattices forms them. In particular, the sharp peak at 43.45° confirms the high degree of nanocrystallinity of the material. The XRD peaks at 16.35° and 43.45° confirm the existence of new, complex crystallographic phases formed exactly from the interaction of these elements. The XRD peaks at 43.45° and 44.85° correspond to the B2 (austenite) or B19' (martensitic) phases in the Ni-Ti system [14]. This determines the material's mechanical memory and high-strength properties.

The low-intensity reflections in the $2\theta = 50^\circ - 70^\circ$ range, namely at angles of 50.35°, 58.55°, 61.05° and 67.45°, are higher-order secondary peaks of the main Ni-Ti and Ni_3Ti phases. Their presence indicates that the crystal lattice possesses long-range order, meaning the material is uniformly crystallized throughout its entire volume. Thus, the system is not a simple Ni-Ti as expected, but rather a doped multi-phase intermetallic composite. The fact that Nd and Zr elements have formed a new stable structure in the 16.35° region may serve to improve the thermophysical properties of the material.

The Full Width at Half Maximum (FWHM) of the peaks and the low background (red line) indicate that the material consists of highly dispersed crystals with low defect density. Particularly in the 16.35° and 20.05° regions, the sharp and narrow nature of the peaks indicates that the crystallite sizes are homogeneous. This can be demonstrated by the following Scherrer formula:

$$D = \frac{K\lambda}{\beta \cos\theta} \tag{1}$$

To validate the particle size observations, the crystallite size (D) was calculated using the Scherrer equation, based on the primary XRD peaks of the Ni-Ti B2 phase. The calculated average crystallite size was found to be approximately 22 ± 5 nm. A comparison with TEM images, which show physical particle diameters between 20 and 60 nm, indicates that the nanoparticles are either polycrystalline or possess a "core-shell" structure where a crystalline intermetallic core is enveloped by a thin amorphous oxide layer. This correlation confirms that the spark discharge method promotes high crystallinity within the core despite the rapid quenching in the electrolyte.

TABLE I: Comparison of crystallite size (XRD) and particle size (TEM).

Phase	2θ (deg)	Crystallite Size (Scherrer, nm)	Particle Size (TEM, nm)
Ni-Ti (B2)	16.35	24.2	20 – 60
Ni_3Ti	20.5	18.5	20 – 60

The most intense peaks in the XRD pattern correlate with the predominance of the NiO phase (71.17%) within the composition. The extremely high intensity suggests the presence of preferred crystal growth (texturing) in a specific direction within the sample. As confirmed by the sharp doublet peaks in the 58.55° and 61.05° regions, the spark discharge in the aqueous medium has formed a stable and ordered oxide framework. The low background level proves that all components were fully crystallized under the influence of the plasma.

Furthermore, the XRD analysis results indicate that the added dopants (V, Zr, Nd) did not form separate independent phases but were successfully incorporated into the primary Ni-Ti oxide matrix lattice in the form of a solid solution. This process can be explained through Vegard's law. The difference in cationic radii, where Ni^{2+} = 0.69 Å and Nd^{3+} = 0.98 Å, caused changes in the crystal lattice parameters and led to the emergence of internal lattice strain. The slight shift and broadening of the peaks are precisely the result of this structural deformation, which forms a "defect structure" that enhances the catalytic activity of the material.

Here, the influence of Zr on the Ni-Ti system deserves specific mention; in particular, an increase in Zr content leads to a shift in the XRD peaks [15]. Additionally, V plays a significant mechanical and structural role, as its inclusion in the composition

 Copyright © 2025

results in the alteration of lattice parameters and the establishment of stability [16]. Therefore, according to the XRD analysis above, the sample is not merely a mixture of oxides. Instead, it has been scientifically proven to be a highly crystalline, alloyed functional nanocomposite with a complex structure, controlled defects, and a high degree of crystallinity.

The Raman spectrum presented in Figure 4 below reveals crucial information regarding the molecular vibrations and phase composition of the sample.

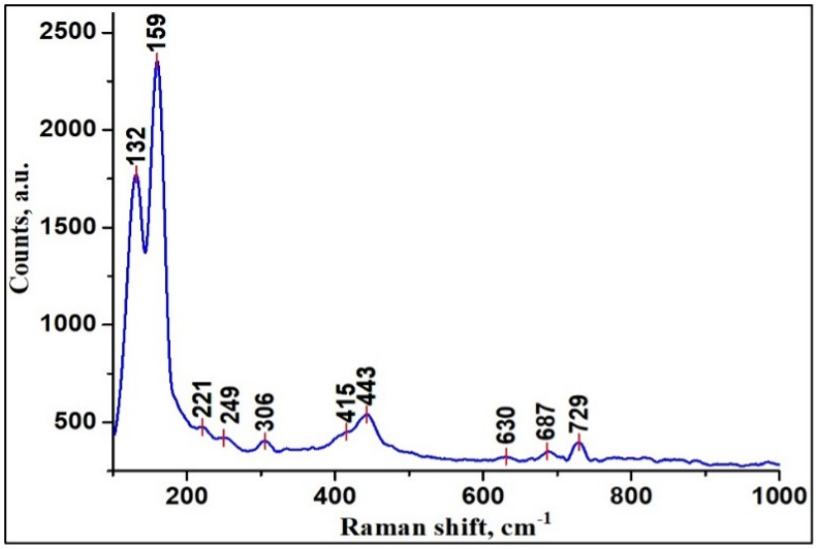


FIG. 4: Raman analysis of the sample

This spectrum analysis correlates almost perfectly with the previous XRD results. Several distinct peaks are observed in the spectrum, acting as the molecular "fingerprints" of the primary and secondary phases within the sample. The low-frequency dominant peaks at 132 cm^{-1} and 159 cm^{-1} exhibit the highest intensity and are primarily characteristic of the Ni-Ti system and the anatase phase of TiO_2 [17]. The presence of Ti phases identified in the XRD is further confirmed by these peaks.

Additionally, the 132 cm^{-1} and 159 cm^{-1} Raman peaks indicate surface oxidation of the nanoparticles. Research has shown that the low-frequency lattice phonon modes of TiO_2 and ZrO_2 manifest precisely in the 140–150 cm^{-1} region [18]. This suggests that the surface of the nanoparticles is covered with a passivated oxide layer, confirming a core-shell structure where the core consists of the metallic alloy and the shell is composed of metal oxides [19].

The broad peak in the mid-range at 443 cm^{-1} corresponds to the vibrations of Ni-O bonds or the E_g mode of TiO_2 in the rutile phase. This provides molecular-level evidence of the high concentrations of nickel and titanium in the initial composition. The relatively weaker peaks at 221, 249, and 306 cm^{-1} are associated with the lattice modes of V_2O_5 or $NiTiO_3$ within the sample. The minor peaks at 630, 687, and 729 cm^{-1} primarily represent metal-oxygen-metal (M-O-M) bridging vibrations, confirming the presence of a well-formed oxide framework.

The sharpness of the peaks in the Raman spectrum, particularly at 159 cm^{-1}, reaffirms the high degree of crystallinity previously indicated by the XRD results. The absence of a broad "hump" in the 1000 cm^{-1} region of the spectrum suggests a low content of free water, yet points to the presence of hydroxide groups integrated into the crystal structure, consistent with the XRD findings.

The presence of elements such as V, Zr, and Nd has caused a slight elevation of the Raman baseline and the broadening of the primary oxide peak at 443 cm^{-1}, which is a direct result of internal structural defects and strains. Consequently, the Raman spectrum fully confirms that the sample is not merely a collection of simple oxides, but a doped functional nanocomposite with complex molecular bonding. It possesses a metallic core and a metal oxide shell—primarily composed of TiO_2 (anatase) and NiO phases.

CONCLUSION

In this study, complex multi-component nanoparticles in the Ni-Ti-V-Zr-Nd system were successfully synthesized using the spark discharge method in an aqueous NaCl electrolyte. According to the XRD analysis, the material consists of a highly crystalline intermetallic core, namely Ni-Ti B2 and Ni_3Ti phases, where the Nd and Zr additions induced micro-deformations within the crystal lattice. The retention of all alloying elements (V, Zr, Nd) in the final composition indicates that the inter-element stoichiometric balance was successfully maintained during the synthesis process. Raman spectroscopy results, specifically the

Copyright © 2025

TiO_2 vibrations in the 132 and 159 cm^{-1} regions and Ni-O vibrations at 443 cm^{-1}, confirm the formation of a highly passivated oxide shell on the surface of the nanoparticles, proving the core-shell structure of the material. Optical imaging and XRD data show that the primary particles are in the 20–60 nm size range, while the low background noise level demonstrates the formation of a perfectly ordered nanostructure, free of amorphous phases, under the influence of the plasma. The synergistic effect of electrolyte conductivity and cavitation energy ensures stoichiometric stability.

REFERENCES

[1] Miracle, D. B., Senkov, O. N. (2017). "A critical review of high entropy alloys and related concepts." Acta Materialia, 122, 448-511.

[2] Saburi, T. (1998). "Ti-Ni shape memory alloys." In Shape Memory Materials. Cambridge University Press, 49-97.

[3] Cantor, B., et al. (2004). "Microstructural development in equiatomic multicomponent alloys." Materials Science and Engineering: A, 375, 213-218.

[4] Yeh, J. W., et al. (2004). "Nanostructured high-entropy alloys with multiple principal elements: novel alloy design concepts and outcomes." Advanced Engineering Materials, 6(5), 299-303.

[5] Tunçay, B., Çuğ, H., Tunçay, T., Cesarz-Andraczke, K., Özyürek, D. (2025). Impact of Zirconium Content on Phase Structure and Corrosion Properties of NiTi-Based Shape Memory Alloys. Journal of Materials Engineering and Performance, 1-11.

[6] Markus, A. A., Parsons, J. R., Roex, E. W., de Voogt, P., Laane, R. W. (2016). Modelling the release, transport and fate of engineered nanoparticles in the aquatic environment–a review. Reviews of Environmental Contamination and Toxicology Volume 243, 53-87.

[7] Grasso, D., Subramaniam, K., Butkus, M., Strevett, K., Bergendahl, J. (2002). A review of non-DLVO interactions in environmental colloidal systems. Reviews in Environmental Science and Bio/Technology, 1(1), 17-38.

[8] Tabrizi, N. S., et al. (2009). "Generation of nanoparticles by spark discharge." Nanoparticle Research, 11, 315-332.

[9] Suryanarayana, C. (2001). "Mechanical alloying and milling." Progress in Materials Science, 46(1-2), 1-184.

[10] Barcikowski, S., Compagnini, G. (2013). "Advanced nanoparticle generation by laser ablation in liquids." Physical Chemistry Chemical Physics, 15(9), 3022-3026.

[11] Cushing, B. L., et al. (2004). "Recent advances in the liquid-phase syntheses of inorganic nanoparticles." Chemical Reviews, 104(9), 3893-3946.

[12] Zaripov, A., Khudaykulov, I., Ashurov, Kh. (2025). Spark discharge in a liquid medium as an effective method for synthesis of nanoparticles of multi-element composites with controlled dimensions and morphology. Physics and chemistry of materials treatment. 4. 53-60.

[13] Tofail, S. A. M., Butler, J., Gandhi, A. A., Carlson, J. M., Lavelle, S., Carr, S., Tuissi, A. (2014). X-ray visibility and metallurgical features of NiTi shape memory alloy with erbium. Materials Letters, 137, 450-454.

[14] Otsuka, K., Ren, X. (2005). "Physical metallurgy of Ti–Ni-based shape memory alloys." Progress in Materials Science, 50(5), 511-678.

[15] Ramos, A. P., Castro, W. B. D., Costa, J. D., Santana, R. A. C. D. (2019). Influence of zirconium percentage on microhardness and corrosion resistance of Ti50 Ni50-xZrx shape memory alloys. Materials Research, 22(4), e20180604.

[16] He, Z., Liu, M. (2011). Effect of heat treatment on transformation behavior of Ti–Ni–V shape memory alloy. Materials Science and Engineering: A, 528(22-23), 6993-6997.

[17] Sedigh Rahimabadi, P., Khodaei, M., Koswattage, K. R. (2020). Review on applications of synchrotron-based X-ray techniques in materials characterization. X-Ray Spectrometry, 49(3), 348-373.

[18] Frank, O., Zukalova, M., Laskova, B., Kürti, J., Koltai, J., Kavan, L. (2012). Raman spectra of titanium dioxide (anatase, rutile) with identified oxygen isotopes (16, 17, 18). Physical Chemistry Chemical Physics, 14(42), 14567-14572.

[19] Salgueiriño-Maceira, V., et al. (2006). "Composite silica spheres with magnetic and luminescent functionalities." Advanced Functional Materials, 16(4), 509-514.

 Copyright © 2025